Automatic Virtual Impedance Adaptation of a Knee Exoskeleton for Personalized Walking Assistance

Prudhvi Tej Chinimillia, Zhi Qiaoa, Seyed Mostafa Rezayat Sorkhabadia, Vaibhav Jhawara, Iat Hou Fonga, Wenlong Zhanga,

^aRobotics and Intelligent Systems Laboratory, The Polytechnic School, Ira A. Fulton Schools of Engineering, Arizona State University, Mesa, AZ, United States.

Abstract

This paper attempts to address the problem of online modulation of virtual impedance for an assistive robot based on real-time gait and activity measurements to personalize the assistance for different users at different states. In this work, smart shoes and inertial sensors are introduced to measure ground contact forces and knee joint kinematics, respectively. An automatic impedance tuning (AIT) approach is presented for a knee assistive device (KAD) based on real-time activity recognition and gait phase detection. The activities considered in this paper are level, uphill, and downhill walking. A Gaussian mixture model (GMM) is employed to map the fuzzy likelihood of various activities and gait phases to the desired virtual impedance of the KAD. The prior estimate of virtual impedance is defined using human knee impedance identified with the walking data collected on different users. The AIT approach is integrated into the high-level impedance-based controller of the KAD for assistance during the stance phase. Finally, to evaluate the benefit of the proposed algorithm in stance phase, an EMG sensor is placed on the vastus medialis muscle group of three participants. The proposed approach is compared with two baseline approaches: constant impedance and finite state machine, and the results demonstrate that the profiles of impedance parameters and robot assistive torque are smoother and the muscle activity of vastus medialis is reduced. It is also noticed that the participants reduce their step lengths and increase walking cadence with assistance from the KAD.

Keywords: Wearable sensors, Assistive robotics, Human intention estimation, Impedance control, Rehabilitation

1. Introduction

The world is witnessing a significant and unprecedented demographic shift with more than 20% of the U.S. residents projected to be 65 or older by 2030, compared to 13% in 2010 [1]. Aging leads to impaired mobility due to degenerative conditions of the musculoskeletal system, the cardiovascular system, and the nervous system. With more people suffering from mobility issues, it is not enough to apply only conventional treatment and rehabilitation technologies, which are expensive and limited to hospitals [2].

In observation of such challenges, wearable sensors and robotics have attracted significant attention in recent years. They have shown great potentials in improving our understanding of gait abnormalities, reducing labor intensity for therapists, and enabling home-based tele-rehabilitation [3, 4]. For human walking analysis, encoders and inertial sensors have been employed for studying walking kinematics [5]; force plates and force sensor embedded insoles have been used to study the ground contact forces (GCFs) in various gait phases [6]; electromyography (EMG) sensors have been used to analyze

muscle activities during walking [7]. Various machine learn-

Existing research on wearable robots has paved the way for providing safe and accurate assistance to improve the training performance. From the design perspective, series elastic [10], cable-driven [11], and variable stiffness [12] mechanisms have been developed to make the wearable robots lightweight, affordable, and adaptive. In contrast to rigid-link robots, soft robotics has been an emerging area in recent years. Soft robots are lightweight, inherently safe, and compliant, which make them an ideal candidate for wearable assistance [13].

The proper assistance of wearable robots significantly depend on planning and control. For motion planning of the wearable robots, impedance control has been the most popular approach due to its simple implementation and clear physical intuition [14]. Over the years, the finite state machine (FSM) is a widely adopted strategy to modulate the impedance parameters in the robot controller based on gait phases and activities. To implement FSM, it becomes important to integrate the realtime gait and activity detection algorithms into the high-level control of the assistive robot. Hybrid Assistive Limb (HAL3) is a famous lower-extremity wearable robot. It broadly classified one walking cycle into support and swing phases based on force resistive sensor threshold, and constant torque is applied to hip and knee joints [15]. Apart from HAL, other companies

Email addresses: Prudhvi.Chinimilli@asu.edu (Prudhvi Tej Chinimilli), zqiao7@asu.edu (Zhi Qiao), srezayat@asu.edu (Seyed Mostafa Rezayat Sorkhabadi), Vaibhav.Jhawar@asu.edu (Vaibhav Jhawar), ifong@asu.edu (Iat Hou Fong), Wenlong.Zhang@asu.edu (Wenlong Zhang)

ing approaches, such as support vector machine [8] and hidden Markov model [9], have been applied to process the wearable sensor data automatically and extract useful insights for decision making.

Existing research on wearable robots has payed the way for

^{*}Corresponding author.

such as ReWalk [16] and Ekso Bionics [17] built hip-knee exoskeletons and employed FSM controller strategy to assist individuals with SCI. In [18], a FSM based controller is designed for five gait phases to allow variation in impedance for the knee joint. The gait phases are detected based on knee angles and manually defined thresholds of GCFs. A FSM controller is implemented in [19], in which the stiffness of the knee actuator is modulated based on stance and swing phases of the gait cycle. In MINDWALKER exoskeleton, a FSM based impedance controller is designed for nine states in a gait cycle [20]. A FSM based impedance controller is implemented for modulating impedance parameters in the robotic device with knee and ankle actuators for sitting, standing and walking activities in [21], and for stair ascent and descent in [22]. Although FSM has shown promising results, there still remains a major limitation, as it leads to discrete jumps in the impedance parameters during state transitions [20, 23].

In the aforementioned work, the impedance parameters are manually set for different gait phases or activities which requires a lot of time and experience from medical professionals. Moreover, these parameters may differ across users. Therefore, it is not possible to design generalized impedance parameters profile across the users, instead, they need to be personalized based on user's requirements. To address these issues, researchers started focusing on the human joint impedance studies to get more insight on the joint impedance modulation, and to design the assistive robots that mimic the physiological joint behavior [24]. The conventional methods to determine joint impedance involve perturbing the joint in a controlled manner, and describing impedance as the dynamic relationship between applied perturbations and corresponding joint torques [25]. Some developed methods to estimate the elastic components of the knee joint impedance that depends on muscle activation [26]. Others modeled the knee joint as a spring-damper system and identified knee stiffness, damping and setpoint for gait phases [27]. The results from the aforementioned human studies demonstrated that the human modulates the impedance parameters in a smooth and continuous manner within a gait cycle and these impedance parameters profile changes from subject to subject. Despite ongoing research on human joint impedance studies, there still exists a gap in embedding those insights into impedance-based controller strategy for robots.

Inspired by the aforementioned limitations of the existing work, the main focus of this paper is to provide smooth impedance modulation for the robotic assistive device to assist the user in a personalized manner. This is approached by imparting the identified impedance parameters in human study experiments to the robot controller. An automatic impedance tuning (AIT) algorithm is proposed which automatically modulates the impedance parameters for gait phases and activities. Smart shoes and inertial sensors are introduced to collect GCF and kinematic data. Activity recognition and gait phase detection algorithms are developed to understand human walking in real time. These algorithms provide fuzzified values instead of deterministic decisions. These fuzzy likelihood values provide flexibility for smoothing the impedance parameters profile. A Gaussian mixture model (GMM) is trained to map the

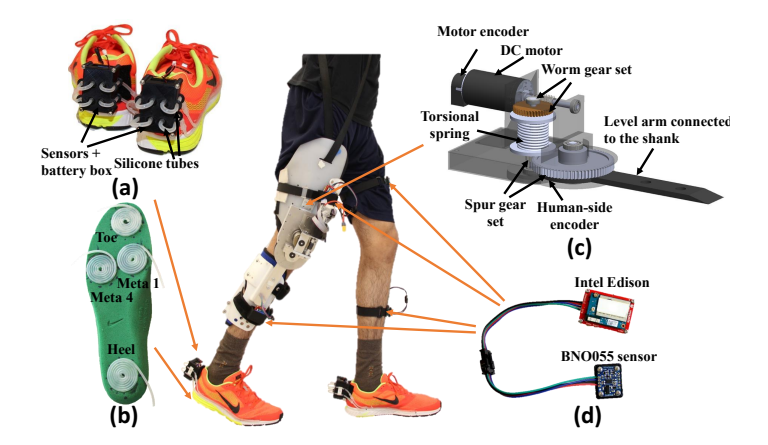


Fig. 1. Wearable sensing system and knee assistive device (KAD).

fuzzy likelihood of activities and gait phases to the desired virtual impedance of the robot, based on the identified user knee impedance for different activities and gait phases.

The scope of this paper is to provide assistance during stance and implement zero impedance case to allow user free motion during swing. The contributions of this paper include:

- 1. An online activity and gait phase detection approach is developed based on force and kinematic data
- 2. An automatic online impedance tuning approach is developed based on human knee characterization and GMM to allow smooth transitions and personalize the assistance
- 3. The efficacy of these algorithms is verified by experiments with three human participants and its potential benefit is illustrated using kinematics and EMG metrics

The remainder of this paper is organized as follows. Section 2 discusses the mechatronic design of the wearable sensors and assistive robot. In Section 3, the human knee impedance is studied. Section 4 introduces the activity and gait phase detection algorithms. The online impedance tuning algorithm is discussed in Section 5. Experimental results with three participants are presented in Section 6. In Section 7, the experimental results are discussed and the potential of the AIT approach in clinical applications is detailed. Section 8 concludes this paper and presents future work.

2. Mechatronic design

2.1. Wearable sensing system

The wireless wearable sensing system comprises inertial measurement units (IMUs) and smart shoes to measure knee joint angles and GCFs. The system is connected to a high-performance computer through a stable wireless ad-hoc network using the TCP/IP protocol. The smart shoes are developed to measure GCFs at four points: heel, first metatarsal joint (Meta 1), fourth metatarsal joint (Meta 4) and toe while the silicone tubes are wound into air bladders and connected to barometric pressure sensors shown in Fig.1(a) and (b). The sampling rate of the smart shoes is set to 100 Hz and a model-based

Table 1 Design specifications for components of KAD.

Component	Specification	Value	
Torsion spring	Spring constant Max angular deflection	6.59 N·mm/deg 317 degrees	
Worm gear	Gear ratio Pressure angle Lead angle	10:1 25 degrees 18.26 degrees	
Spur gear	Gear ratio Pressure angle	6.36:1 14.5 degrees	
Encoders	Resolution	2000 counts/turn	

filter is implemented to compensate for hysteresis and estimate GCFs from pressure sensor readings in real time [28].

Four IMUs are placed on bilateral thighs and shanks to measure acceleration and angular rate in real time. The placement of IMUs on the participant is shown in Fig.1. The combined Bosch Sensortec's BNO055 IMU and an Intel Edison processor is used for motion sensing, as shown in Fig.1(d). The sampling rate of all IMUs is set to 100 Hz. The knee angle is estimated by initially aligning the sensor frames of thigh and shank using functional alignment procedure and then calculating the relative orientation using an extended Kalman filter [29].

2.2. Knee assistive device (KAD)

A knee assistive device (KAD) is an exoskeleton with a compact rotary series elastic actuator (cRSEA) [10]. In a cRSEA, a worm gear and spur gear combination is used to amplify and change the direction of assistive torque generated by a DC motor. The mechanical design of KAD is shown in Fig.1(c). The cRSEA is compact and light with a weight of 1.57 kg to avoid unbalance and discomfort to users. The maximum power consumed by the knee joint is about 80W for a male subject with the body weight of 70 kg and during level walking and the knee angular velocity ranges between ±60 rpm [10]. Considering this, Maxon RE40, a 150W DC Motor is used to power the KAD. With a combined gear set reduction ratio of 63.6:1, the end effector can reach a maximum angular velocity of 120 rpm and the KAD can provide a maximum continuous assistive torque of 11.26 N·m. Two incremental optical rotary encoders (US Digital) are used to measure both motor and human knee angles, which are re-initialized at the beginning of each experiment. The torsion spring serves as a torque sensor and also provides an energy buffer to prevent injuries from unexpected high motor torques. The specifications of the components used in the KAD are given in Table 1. The design of KAD targets people with unilateral impairment which affects knee function. In this paper, the KAD is used to assist right side knee.

3. The study of human knee motion

In a gait cycle, human continuously modulates their joint impedance depending on the activity, speed, and terrain. The understanding of human joint impedance helps to design virtual

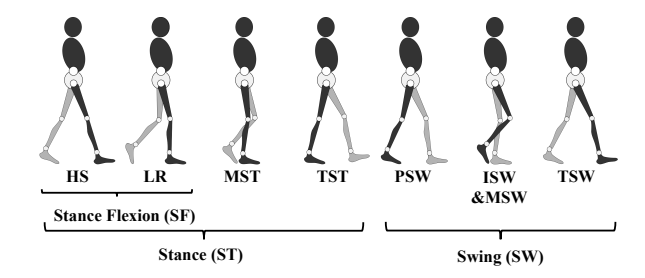


Fig. 2. The gait cycle of human walking. HS - heel strike, LR - loading response, MST - mid stance, TST - terminal stance, PSW - pre-swing, ISW - initial swing, MSW - mid swing, and TSW - terminal swing.

 Table 2

 The details of healthy participants volunteered for the experiments.

ID	Gender	Age	Height (cm)	Weight (kg)
1	Male	22	180	59.96
2	Male	31	183	77.61
3	Female	26	158	55.01

impedance of the assistive robot. There are two objectives associated with performing experiments: 1) to get the knee kinematics and kinetics data to study human impedance modulation and to identify the parameters of the model that will be discussed in Section 3.2. 2) To get the experimental data to train GMM in AIT algorithm that will be proposed in Section 5.1.

3.1. Experimental setup

The experiments were set up in the motion capture laboratory which was equipped with 12 high-speed infrared cameras (Vicon Motion Systems Ltd.,) and instrumented treadmill (Bertec Corporation) at Arizona State University (ASU). The ASU Institutional Review Board (IRB) reviewed and approved this study. The details of the healthy participants volunteered in the experiments are given in Table 2. The speed of the treadmill was set to 0.8 m/s for the level walking and 0.6 m/s for both uphill and downhill walking. The slope of the treadmill was set to 0, +10, and -10 degree for level, uphill, and downhill walking. There is a limitation related of the instrumented treadmill that it does not allow changing the slope while running. Therefore, the experiments of three activities were planned separately without focusing on their transitions. A total number of 9 experimental sessions were conducted on each participants allocating three sessions for each walking activity. Each session lasted for 1 minute. The participant relaxed for 2 to 3 minutes in between the sessions within an activity and for 15 minutes before starting other activity sessions.

For the experiments, participant worn 16 markers, 4 IMUs, and smart shoes. The Vicon camera captures markers at a frame rate of 100 Hz. The plug-in gait Vicon software registers lower body joint angular displacements and computes gait parameters such as cadence and step length. Also, the knee moment is calculated by the Vicon software which takes moments from instrumented treadmill and marker's position as inputs. The joint moment is estimated by applying inverse dynamics to the multi-body model given in [30].

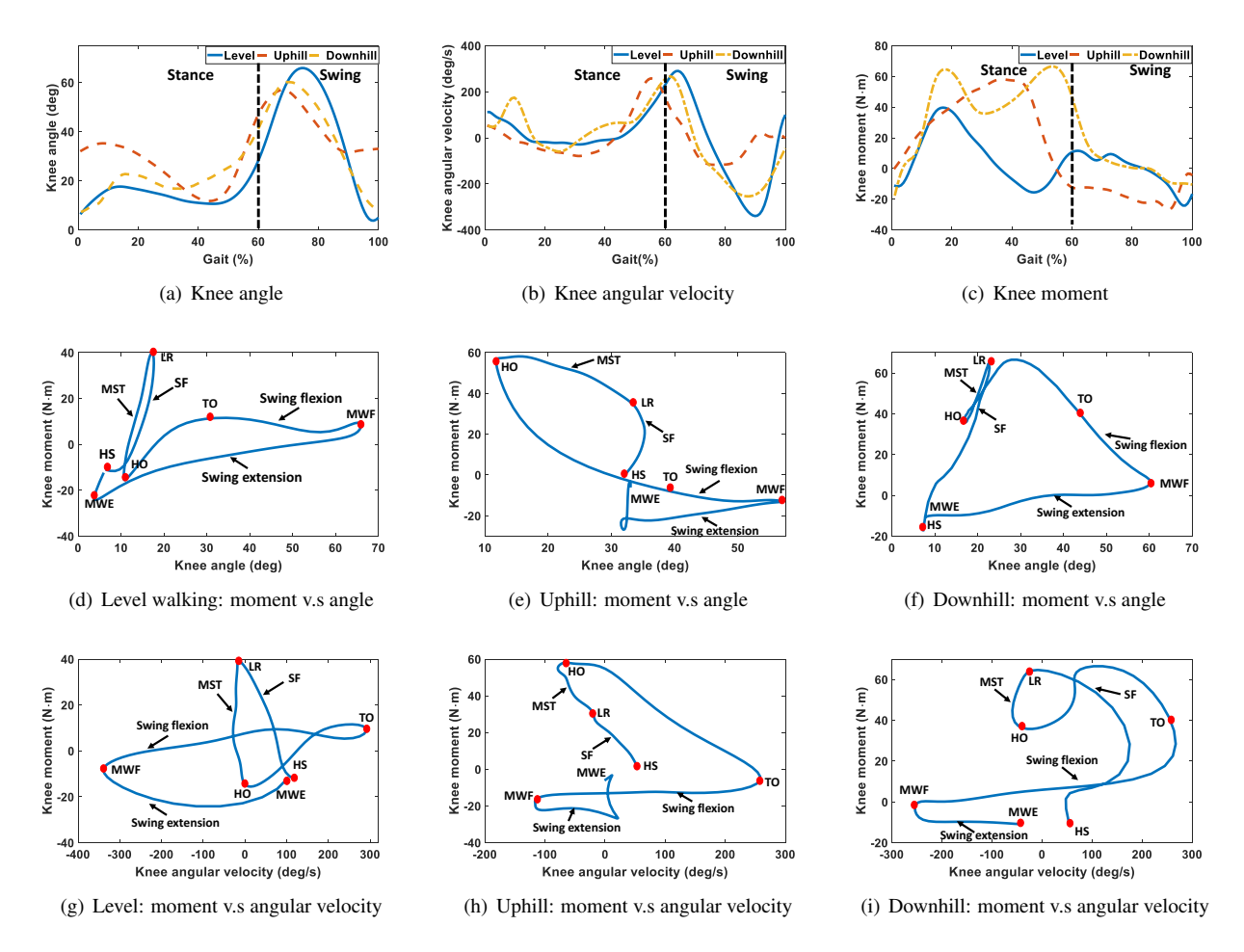


Fig. 3. The comparison of knee kinematics and kinetics of one gait cycle for three activities experiments performed on participant 1. The slope of the treadmill was set to 0, +10, and -10 degree and the speed of the treadmill was 0.8 m/s, 0.6 m/s, and 0.6 m/s for level, uphill, and downhill walking experiments.

3.2. Human knee impedance model

This paper primarily focuses on identifying the knee stiffness and damping during the stance phase for three activities. A spring damper model is considered for modeling the human knee torque with respect to the knee angle and angular velocity [27]. The kinematics and kinetics data are processed for the right knee as our KAD is designed for right side. The spring damper model is defined as [27]:

$$T_h(t) = k \cdot (\theta_h(t) - \theta_0) + b \cdot \dot{\theta}_h(t), \tag{1}$$

where $T_h(t)$, $\theta_h(t)$, and $\dot{\theta}_h(t)$ are the human knee torque, angle, and angular velocity, respectively. k, b, and θ_0 represent the knee stiffness, damping, and setpoint, respectively. A gait cycle can be divided into two main phases: stance (ST) and swing (SW). The ST can be further divided into three subphases: stance flexion (SF), mid stance (MST) and terminal stance (TST), as shown in Fig.2. The SF phase includes the heel strike (HS) and loading response (LR). In this paper, k, b, and θ_0 are identified for three phases SF, MST, and TST using a least square method with $T_h(t)$ as output and $\theta_h(t)$, $\dot{\theta}_h(t)$ as inputs. The identified mean and standard deviation of k, b and θ_0 for three participants for a minute are given in Table 3.

3.3. Discussion

The knee angle, angular velocity, and moment for the activities of participant 1 are shown in Figs. 3(a) - 3(c). The knee moment versus angle and knee moment versus angular velocity during one gait cycle for different activities are shown in Figs.3(d) - 3(i), and it can be seen that the SF takes place from HS to LR. Whereas, MST is from LR to heel off (HO) and the TST is up to toe off (TO). The swing knee flexion is observed from TO to maximum swing flexion (MWF) and swing knee extension takes place up to the next HS. The knee flexion during HS is higher for uphill in comparison with the level or downhill walking which can be seen in Fig.3(a). The knee plays a wide range of roles during the execution of the gait, including supporting the body weight and deceleration during stance by applying a large knee moment that can be seen in Figs. 3(g) - 3(i). The knee undergoes a resistive flexion during SF and a propulsion extension during MST. On the other hand, knee undergoes a ballistic movement demanding a less significant effort during swing phase. This trend is observed in knee moment plots shown in Fig. 3(c).

The knee stiffness follows a more linear profile in the stance compared to swing in three activities shown in Figs. 3(d) - 3(f). It can be seen from Table 3 that maximum stiffness for level and

Table 3 The identified mean and SD of stiffness k (N·m/degree), damping b (N·m·s/degree) and set point θ_0 (degree) for a minute for three participants.

Gait phases	Parameters -	Activities		
Gait phases		Level	Uphill	Downhill
SF	k_{SF}	1.641 ± 0.619	3.580 ± 0.781	4.415 ± 0.382
	b_{SF}	0.035 ± 0.039	-0.070 ± 0.219	-0.052 ± 0.011
	θ_{SF}	9.79 ± 3.376	38.91 ± 2.299	8.826 ± 1.395
MST	k_{MST}	6.058 ± 1.038	2.604 ± 0.773	5.841 ± 1.029
	b_{MST}	-0.215 ± 0.069	-0.151 ± 0.048	0.057 ± 0.023
	θ_{MST}	10.267 ± 1.183	35.393 ± 2.417	22.940 ± 3.778
TST	k_{TST}	0.352 ± 0.287	6.246 ± 1.075	3.0425 ± 0.229
	b_{TST}	-0.308 ± 0.133	-0.369 ± 0.123	-0.080 ± 0.012
	θ_{TST}	0.031 ± 0.029	22.94 ± 3.778	3.702 ± 0.609

downhill walking is observed during MST phase, but for uphill it is observed during terminal stance, which is also shown in the knee angle-moment plots Figs. 3(d) - 3(f). This can be justified from the biomechanical perspective that the instant where the body begins to transit from force absorption at impact to force propulsion happens during MST in level, and downhill walking. Whereas, this transition happens during TST in uphill walking [31]. The knee damping values for the stance phases in three activities are also shown in Table 3. The knee damping values for downhill during MST and TST are relatively high compared to level and uphill walking. This can also be inferred from the knee angular velocity and moment plots shown in Figs. 3(g) -3(i) that the knee moment is higher in downhill compared to other activities during MST and TST. This is consistent with the biomechanical analysis that higher knee moment is exhibited in downhill to account for the negative slope of the contact surface during MST and TST [31].

The identified knee stiffness, damping, and setpoints in the experiments are used in tuning the actuator impedance for the same participant wearing the KAD. The impedance parameters for AIT algorithm in ST phase is set to 10% of the identified impedance exhibited by the participant as shown in Table 3. The percentage value is selected based on the torque limit of the actuator.

4. Human intention estimation algorithm

The overview of the human intention estimation algorithm is shown in Fig. 4. This algorithm utilizes the fuzzy logic method [32] and includes two modules: gait phase detection (GPD) and activity recognition (AR). The GPD module detects four phases in every gait cycle: SF, MST, TST, and SW. In addition to the four phases, the GPD module will provide HS detection as well. Meanwhile, the AR module is used to provide estimation of three activities: level, uphill and downhill walking

4.1. Gait phase detection (GPD) module

The GPD module's fuzzy logic rule base is inspired by [6], where two hyperbolic functions are used as input membership functions while our GPD module's input and output membership functions are changed to partially overlapped trapezoid and triangular functions, as shown in Fig. 5(a) and (b). This change

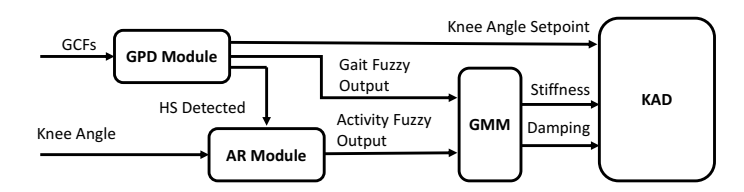


Fig. 4. The overview of AIT algorithm structure.

accounts more samples into the gait phase transition period instead of a specific gait phase and provides a smoother gait fuzzy output profile, shown in Fig. 6. Once a new gait phase is detected by the GPD module, the value of the knee setpoint will change correspondingly. Also, the outputs of this module will be used as part of the training data set for GMM and the input to AIT which is discussed in Section 5.

4.2. Activity recognition (AR) module

An fuzzy inference algorithm was developed in our previous work that can detect six activities in real time [33]. The algorithm is based on the knee angle and GCF measurements from IMUs and smart shoes. The design of the rule base in Table 4 is inspired by the human walking patterns, shown in Fig. 3(a). It is obvious that during the SF phase, the right side knee angle is larger in the uphill case compared to the other two activities. This difference brings the definitions of high and low in the rule base for right side. Once the rule base is built, the input and output fuzzy logic membership functions are defined using trapezoid functions. The max method of aggregation and centroid method of de-fuzzification is used to generate a final fuzzy output [33]. Like the output from GPD module, this fuzzy output value will be used in impedance tuning algorithm. However, limited by the treadmill, the module is simplified to detect three activities: level, uphill, and downhill walking. To make it clear, this module will only be activated when the right side HS is detected by GPD module and the output will be kept until the next right HS happens. For three participants, the ranges of the activity fuzzy output values defined for level, uphill, and downhill walking are 0–0.3, 0.31–0.6, and 0.61–1, respectively.

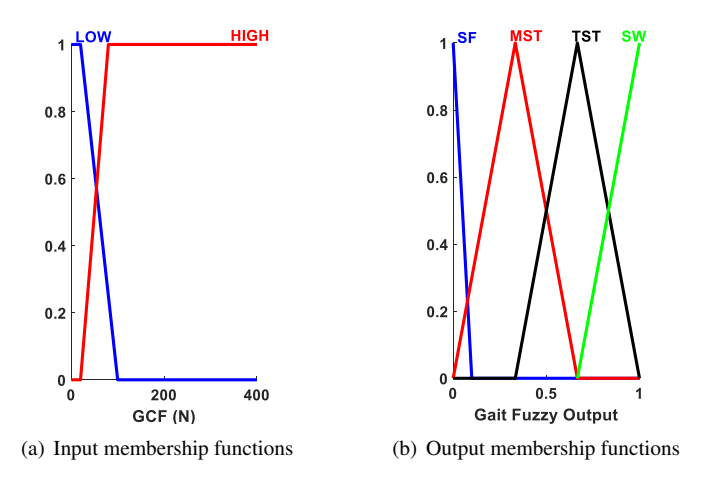


Fig. 5. Example of the input and output membership functions of the GPD module

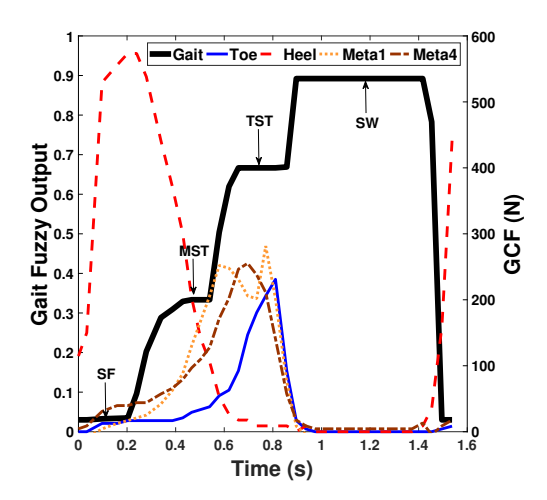


Fig. 6. The result of the GPD module for a gait cycle of participant 1. Gait (bolded in black) indicates the output of GPD module whose range varies from 0 to 1 (unit less). Toe, Heel, Meta1 and Meta4 are the inputs.

Table 4 The rule base for activity detection with θ_R (right) and θ_L (left) knee angles.

Activity	θ_R	θ_L
Level walk	low	medium
Uphill	high	low
Downhill	low	high

5. Automatic impedance tuning (AIT) algorithm

The AIT algorithm is an online impedance tuning algorithm which tunes the virtual stiffness and damping values based on the fuzzy outputs from GPD and AR modules. In AIT, a GMM is trained with the gait and activity fuzzy output values obtained from the participant's walking experiments. The training dataset of a healthy participant is shown in Fig. 7 in which gait and activity fuzzy values are plotted on x and y axes, respectively. It can be seen from Fig. 7 that fuzzy values along y axis is more separated compared to x axis, since the training data does not contain transitions among the activities.

5.1. Gaussian mixture model (GMM)

The GMM is a parametric probability density function represented as a weighted sum of Gaussian component densities. In this paper, three activity components (level, uphill and downhill walking) and four gait phase components (SF, MST, TST, and SW) are separately defined on y axis and x axis which forms a 3 by 4 Gaussian components group. The Gaussian component is labeled as C_{ij} where i and j represents the activity and gait phase components respectively. Meanwhile, the outputs from GPD and AR modules are labeled as q_1 and q_2 , respectively. Using the Expected Maximization (EM) method, the parameters of the GMM are identified from the training data [34]. A given new data point (q_1,q_2) firstly generates a feature vector $\mathbf{q} = [q_1,q_2]^T$. Then, the probability of this data belonging to

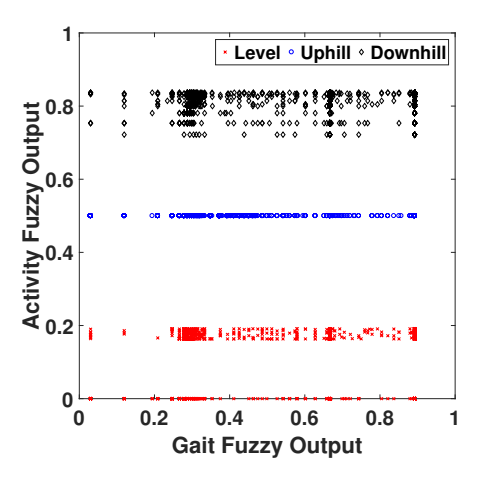


Fig. 7. The training data set for GMM with participant 1. The participant walks at the speed of 0.8 m/s on the level surface and 0.6 m/s on 10 deg uphill/downhill condition. The Gait and Activity fuzzy outputs range from 0 to 1 and are calculated through GPD and AR module, respectively.

Algorithm 1 AIT

Input: l_1, l_2, l_3, l_4 : GCF for heel, Meta 1, Meta 4 and toe sensing points, θ_L, θ_R : Left and right knee angle, k_{ij}, b_{ij} : Stiffness and damping values by knee characterization where i and j stand for the activity and gait phase classes, g_0 : Threshold of fuzzy likelihood for HS detection

Output: k, b: desired actuator stiffness and damping value

- 1: $q_2 = 0$ \triangleright AR module initialized with level walking
- 2: **loop**
- 3: $q_1 = GPD(l_1, l_2, l_3, l_4)$ > Gait fuzzy output q_1 updated
- 4: **if** $q_1 < g_0$ **then**
- ▶ HS detected
- 5: $q_2 = AR(\theta_L, \theta_R)$ > Activity fuzzy output q_2 updated
- 6: **else**
- 7: ► HS not detected q₂ = q₂ ► Keep the previous activity detection
- 8: **end if**
- 9: $(k,b) = GMM(q_1, q_2, k_{ij}, b_{ij})$
- ▶ Impedance updated

10: end loop

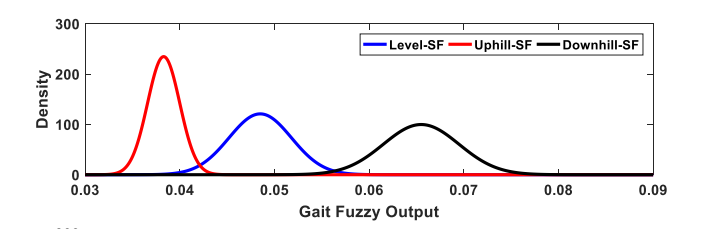
component C_{ij} is given by Bayes rule:

$$p(C_{ij} \mid \mathbf{q}) = \frac{p(C_{ij})p(\mathbf{q} \mid C_{ij})}{p(\mathbf{q})}$$
(2)

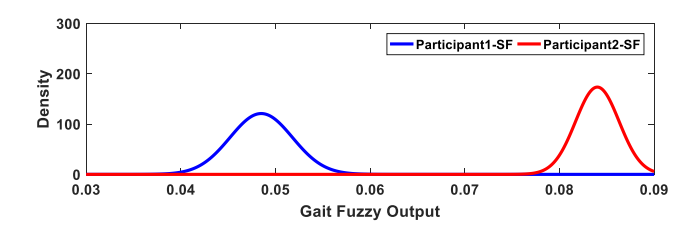
where the prior component weighting factors $p(C_{ij})$ are set to be the same. After the possibility for each component is acquired, the desired actuator stiffness and damping values are calculated as:

$$k = \sum_{i=1}^{3} \sum_{j=1}^{4} p(C_{ij} \mid \mathbf{q}) k_{ij}, b = \sum_{i=1}^{3} \sum_{j=1}^{4} p(C_{ij} \mid \mathbf{q}) b_{ij}$$
 (3)

where k_{ij} and b_{ij} are the identified stiffness and damping values mentioned in Section 3.2, with 3 activities and 4 gait phases, k and b are the actuator stiffness and damping values for the KAD. The AIT algorithm is described in Algorithm 1. Note that the AR module is executed only in the HS phase once every



(a) The SF Gaussian components distribution in different activities for participants.



(b) The SF Gaussian components distribution in level walking for participants.

Fig. 8. Examples of GMM components distribution.

gait cycle, and the algorithm is initiated at level walking activity $(q_2 = 0)$. If the HS is not detected in the next gait cycle, the algorithm will use the last AR module output (q_2) to generate the stiffness and damping values.

In this paper, the algorithm is reduced to a 1D GMM which focuses on the gait phase transition and its performance is verified for three activities level, uphill, and downhill with inclination angles of 0, +10 and -10 degrees. A comparison of GMM components is shown in Fig. 8(a) and (b). As presented in Fig. 8(a), the distributions of SF component in three activities: level, uphill and downhill are different which means, for a single participant, the possibilities that a gait fuzzy output value, i.e. $q_1 = 0.05$ belongs to the SF component are dependent on the activity condition. It is also obvious in Fig.8(b) that, in the same activity condition, the distributions of SF component are distinct between the three participants which indicates the possibility that a given input q_1 belongs to the SF component is dependent on participant as well. These variances in the distributions of the GMM components reflect the individual's walking pattern and make this algorithm personalized to each participant.

5.2. Control structure of KAD

The control structure of KAD includes three layers: impedance planning, torque planning, and motion control as shown in Fig. 9. The AIT approach drives impedance planning layer by providing desired impedance parameters and setpoints. These parameters are then used to calculate the desired assistive torque. There are two ways in the literature to provide the desired knee assistive torque by: 1) using reference knee trajectory for the gait cycle [35], and 2) providing setpoint knee angle conditions for the gait phases [27]. There are limitations associated with the first method as the participant trajectory does not

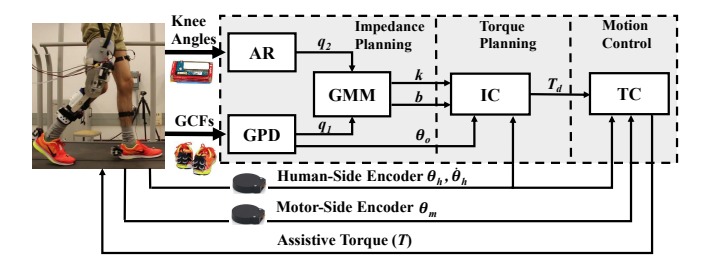


Fig. 9. Control block diagram for the KAD. θ_0 : knee angle setpoint, k: actuator stiffness, b: actuator damping, q_1 : gait phase fuzzy output, q_2 : activity fuzzy output, θ_h : human knee angle, and, $\dot{\theta}_h$: human knee angular velocity. IC: impedance control. TC: torque control. AR and GPD modules are discussed in Section 4.

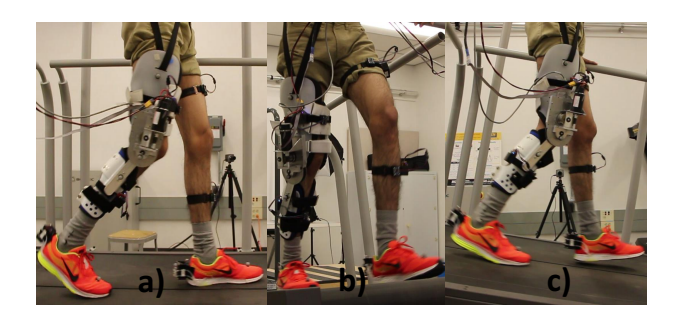


Fig. 10. Experiment setup: a) level, b) uphill, and c) downhill walking.

follow a constant pattern and may deviate from the reference across gait cycles, based on different walking conditions [35]. To avoid this problem, setpoints are defined for each gait phase separately. The desired knee assistive torque follows:

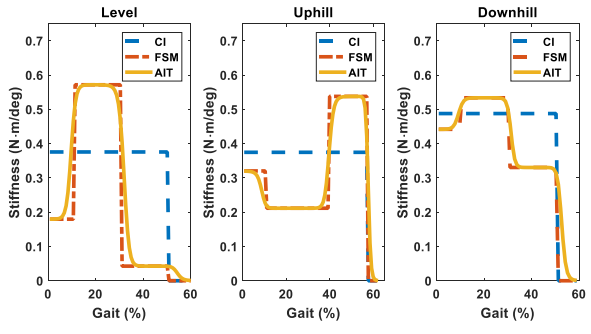
$$T_d(t) = k(\theta_h(t) - \theta_0) + b\dot{\theta}_h(t), \tag{4}$$

where T_d is the desired torque, k and b are the desired actuator stiffness and damping obtained from (3), θ_0 is the setpoint angle which is identified in human study experiments given in Section 3 and determined based on the current gait phase and activity. θ_h is knee angle measurement from human-side encoder.

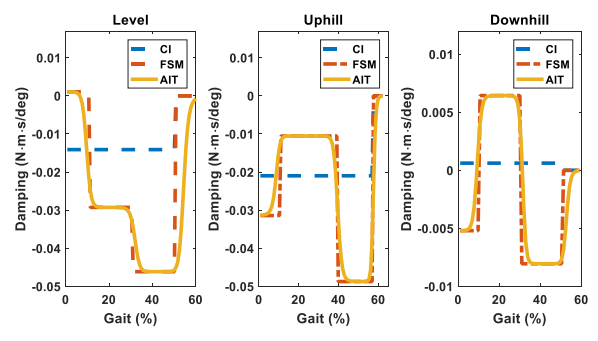
Regarding the rotary series elastic structure of the KAD, the generated torque is proportional to the motor position [10], i.e., the desired torque can be achieved by controlling the motor position in the torque planning layer. Hence, after calculating the torque reference from (4) in torque planning layer, the reference position of the motor is calculated and the motor tracks the reference position using a cascaded PID control loop, in which the inner loop controls the motor velocity and the outer loop controls the position.

6. Experiments and results

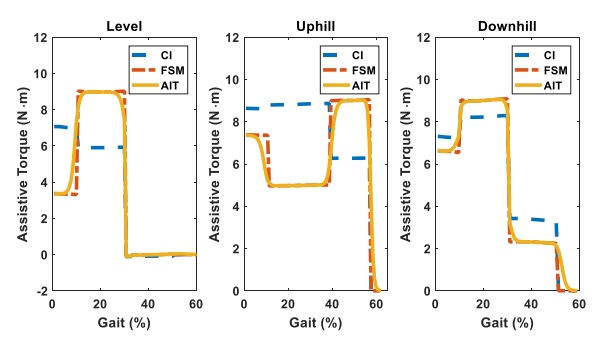
To verify the performance of the AIT algorithm, the same three participants in Section 3 volunteered in the identical experimental setup. The experiment protocol mainly consisted of two cases: passive and active. In passive case, the device was not powered and it did not provide assistance to the participant. Whereas, the KAD provided stance assistance for the knee flexion and extension in the active case. Three types of



(a) Stiffness profile for three activities.



(b) Damping profile for three activities.



(c) Assistive torque profile for three activities.

Fig. 11. The impedance parameters and assistive torque profile in level, uphill, and downhill activities for three cases: CI, FSM, and AIT for participant 1. The x axis in plots represent gait cycle in terms of percentage.

active cases were designed for the experiment protocol: a) constant impedance (CI), b) FSM, and c) AIT. The focus of this section is to compare the performance of the AIT with the two baseline cases: CI and FSM. All the experimental sessions were planned on a single day for a participant. There were five types of sessions proposed: normal walking without KAD, passive, CI, FSM, and AIT cases for each activity. The time duration for sessions and relax time between the sessions was similar to the protocol given in Section 3. Also, the sequence of the sessions were randomized to make them unbiased.

6.1. Impedance and assistive torque

For the implementation of CI and FSM approaches, the gait phase detection outputs need to be deterministic instead of fuzzy. To account for this, the algorithm implemented in [6] was chosen. In the CI case, the impedance was set to a constant predefined value obtained from Table 3 throughout the stance

phase. The impedance was predefined as 10% of the normal impedance exhibited by the participant in FSM case. In the AIT case, the impedance parameters were set as 10% of the impedance obtained from the trained GMM. The desired assistive torque T_d for KAD for gait phases SF, MST, or TST was given by (4). The maximum desired torque for the KAD was set to 9 N·m for all activity sessions as to restrict the actuator from reaching the saturation limit.

The actuator stiffness, damping, and assistive torque for three activities are shown in Fig. 11. The profiles of impedance parameters and assistive torque differ for three active cases. It is clear from Fig. 11 that the AIT case provided smoother impedance parameters and assistive torque profiles, and also smoother transitions between the gait phases in contrast to FSM case. It can been seen from Figs. 11(a) and 11(b) that the stiffness and damping values reaches to zero at nearly 60% of the gait cycle for three activities, which suggests the participant is in swing phase and no assistive torque is provided by KAD. It can be observed from Fig. 11(c) that the knee assistive torque for level walking drops closer to zero at nearly 30% of the gait cycle which is not the case in downhill or uphill walking. The reason is that the stiffness and damping values of the level walking are much lower in TST compared to SF or MST. It should be noted that applying smoothing function, for instance, the sigmoid function to FSM impedance parameters profile can lead to smoother transitions between the states. However, the drawback in such approach is parameters of the sigmoid function need to set manually to account for slope and time shift. In the case of AIT algorithm, the smoother transitions happen due to fuzzy likelihood values obtained from the trained GMM model specific to participant shown in section V. Therefore, the steepness and time shift of the transitions in AIT are participant specific. To compare the performance of proposed AIT with the standard CI and FSM approaches, there is a need to define relevant metrics. The details about the metrics are given in the following subsection.

6.2. Metrics and results

Three types of metrics were chosen for comparison: 1) joint kinematics, 2) gait parameters and 3) muscle activities. For muscle activity comparison, an EMG sensor was attached to vastus medialis as it plays a crucial role in generating knee assistive torque for the stance phase in all the three activities [36].

6.2.1. Joint kinematics and gait parameters

The right knee range of motion (ROM) for the three participants is shown in the Fig. 12 with the mean and standard deviation (SD) for 1 minute during five cases. It is clear from Fig. 12 that the right knee ROM decreases for the active case in comparison to without KAD and passive cases for three activities. The participants exhibited lowest knee ROM in AIT case.

The right side step length was computed as the KAD is designed for right knee assistance. The mean and SD of cadence and the average right side step length for three participants were calculated for one minute shown in the Table 5. It is clear from Table 5 that cadence increases and the step length reduces with

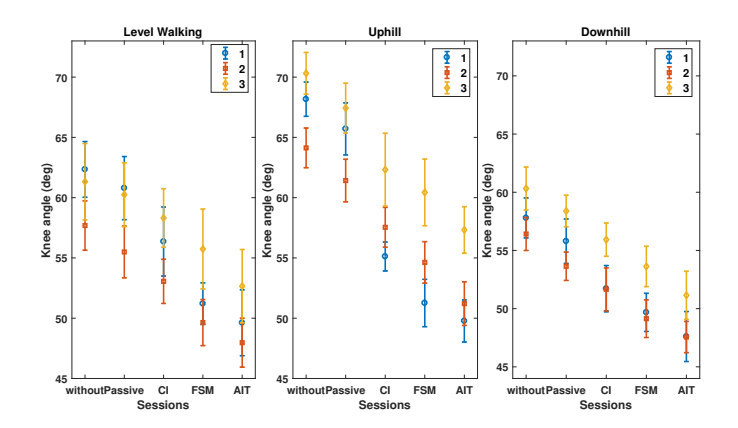


Fig. 12. The mean knee ROM with SD for one minute in three activities for three participants.

Table 5
The mean and SD of cadence (steps/min) and step length (m) for one minute.

Activity	Session	Cadence (steps/min)	Average step length (m)
Level	without	89.18 ± 11.36	0.452 ± 0.097
	Passive	90.69 ± 11.97	0.439 ± 0.096
	CI	92.27 ± 13.98	0.427 ± 0.088
	FSM	93.03 ± 13.71	0.408 ± 0.094
	AIT	93.74 ± 13.98	0.396 ± 0.100
	without	92.62 ± 10.34	0.384 ± 0.029
	Passive	93.86 ± 10.62	0.371 ± 0.031
Downhill	CI	95.24 ± 11.48	0.356 ± 0.024
	FSM	95.67 ± 11.40	0.344 ± 0.030
	AIT	96.82 ± 11.97	0.334 ± 0.033
Uphill	without	78.98 ± 10.51	0.435 ± 0.038
	Passive	80.51 ± 11.41	0.424 ± 0.036
	CI	81.67 ± 11.79	0.415 ± 0.029
	FSM	84.03 ± 13.49	0.403 ± 0.042
	AIT	85.42 ± 14.54	0.393 ± 0.046

assistance. The AIT case exhibited higher cadence and lower step length in all the three activities, which can be inferred from Table 5. The device in passive case adds extra weight to participant's body and lower the performance of walking that is reflected in gait parameters. However, the KAD helps participants spend less effort on the knee joint in active case.

6.2.2. Muscle activity

The maximal voluntary contraction (MVC) experiment on vastus medialis was performed prior to all experiment sessions on each participant to get the reference of the muscle activity. The procedure for MVC experiment was followed as given in [37]. The processing of the EMG signals involves full-wave rectification, detrending, and low pass filtering using 5th order Butter-worth filter [38]. The EMG signals were recorded with a sampling rate of 1000 Hz. Two metrics for muscle activity were chosen: 1) Average EMG activity reduction (P%): first, the average of the peak values of the processed EMG signals

Table 6 The average EMG activity reduction (P%) for one minute in all sessions.

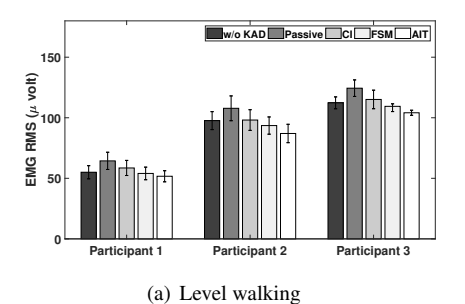
Activity	Session	Participant 1	Participant 2	Participant 3
•	Passive	-11.19%	-8.06%	-10.64%
Level	CI	-4.78%	-1.48%	-2.53%
Level	FSM	1.53%	5.07%	7.89%
	AIT	$\boldsymbol{6.64\%}$	$\boldsymbol{9.27\%}$	11.65%
Downhill	Passive	-8.16%	-6.57%	-9.45%
	CI	-5.17%	1.05%	2.73%
	FSM	1.77%	6.33%	8.15%
	AIT	$\boldsymbol{5.80\%}$	$\boldsymbol{10.99\%}$	$\boldsymbol{12.13\%}$
Uphill	Passive	-6.95%	-9.14%	-8.46%
	CI	-3.40%	-4.82%	2.12%
	FSM	2.69%	2.07%	5.32%
	AIT	8.14%	$\boldsymbol{6.78\%}$	9.65%

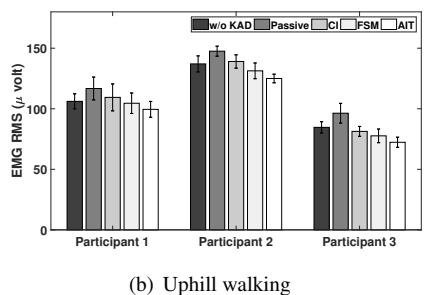
was normalized with respect to MVC value for all five cases; Second, P% was obtained by computing the percentage reduction of those values in passive and three active cases with respect to without KAD case. In conclusion, P% metric gives the measure of change in normalized muscle activation levels in four cases with respect to normal walking. 2) Average root mean square (RMS) of EMG: The RMS of the processed EMG signal with a moving fixed time window is calculated.

The average RMS of the EMG signals with SD during three activities for one minute are reported using a bar chart in Fig. 13. Along with the four cases, without KAD case is included for comparisons. It is clear that the AIT performed best in reducing the average RMS value of the EMG signals. The passive and CI cases showed more average RMS in EMG signals in comparison with without KAD. This can be explained by the weight of the KAD device on the participant. The FSM showed nearly the same or less RMS value compared to without KAD. This can also be verified from P% displayed in Table 6. The passive and CI case showed negative P% which suggests that the normalized EMG value increased in comparison with the without KAD case.

7. Discussion

The KAD assists the participants in stance phase and follows zero impedance strategy during swing phase. It can be seen from the knee angular velocity plot shown in Fig. 3(b) that the swing phase is characterized by high angular velocities. During high angular velocities, the KAD response is increasingly governed by the intrinsic stiffness of the joint which results in resisting torque. Therefore, this alternative assistance and resistance provided by the KAD during stance and swing phases of the gait cycle influences the participants knee ROM. As shown in Fig. 12, the reduced knee ROM is observed in active cases in comparison to passive or without KAD case. Also, the other reason could be that the device introduces inertia and friction due to its weight, which leads to decreased knee ROM. From Table 5, it is clear that the participants exhibited increased cadence and decreased step length. The probable reason can be that as the speed of the treadmill is fixed, the subject need to





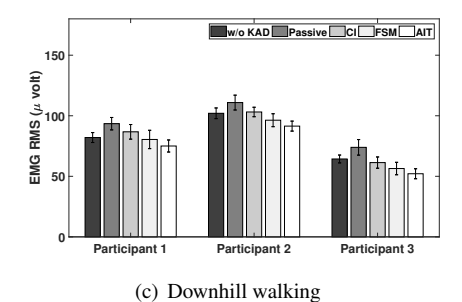


Fig. 13. The mean RMS of EMG signals of vastus medialis with SD measured for a minute in three activities and five sessions, respectively.

compensate for reduced knee ROM with increased cadence. This is confirmed in the study of Aoyagi et al. where the inertia of assistive device results in a reduced range of pelvic motion during zero impedance case [39]. Also, a decrease in knee ROM is observed when walking with LOPES lower limb orthosis in zero impedance case [40]. From the studies [39] and [40], it was shown the reduced joint ROM caused direct effect on gait parameters: step time, step length, and stance time. Also, the subjects showed a tendency to take shorter and quicker steps. As KAD follows zero impedance strategy in swing phase, similar results of reduced knee ROM are observed in this paper.

The percentage improvement of the RMS value of the EMG signals for participant 1 in the AIT case compared to without KAD for level, uphill, and downhill walking are 6.03%, 6.22%, and 8.52%. Whereas, FSM showed 1.8%, 1.4%, and 1.92% improvement. Similarly, for participant 2 and 3, the AIT case exhibited a noticeable improvement in EMG RMS value with respect to without KAD for level, uphill and downhill walking. Similar results can be inferred by looking at *P*% for three participants. The FSM and AIT active cases provided nearly equal assistive torques for gait phases. However, a clear distinction in the muscle activity is observable and AIT performs better than FSM. The possible reason can be that AIT provides smoother impedance and torque profile for the actuator in comparison with the FSM.

7.1. Clinical implications

The approach proposed in this paper addresses the limitations of FSM and provides smooth continuous impedance parameters using the identified human joint impedance. The approach has the potential to become a personalized training system for patients. More experiments need to run to define the impedance parameters for the fuzzy clusters of gait and activity based on the requirements of the patients and the GMM will output the impedance parameters adaptively. As a proof of concept, the knee joint is considered in this paper. It is possible to extend this framework to multiple joints. As the AIT approach provides flexibility in designing the impedance parameters for the clusters of gait and activity, it will be advantageous in clinical settings, as it allows variability in walking pattern, more personalized walking patterns. Also, AIT can provide different impedance parameter profiles, thereby providing various levels of assistance depending on early, mid, and final stages of rehabilitation.

Regarding the effectiveness of this approach in rehabilitation, a clinical protocol with a therapist is needed, in practice, to evaluate the method of automatic impedance modulation and its effect on patients. With this purpose, a graphical user interface (GUI) will be useful for the therapists, in order to facilitate the monitoring of variable such as knee ROM, step length, or cadence and choosing impedance profile.

7.2. Limitations of this study

Due to the limitation of the slope change operation of instrumented treadmill used for the experiments, the transitions between different activities are not evaluated. Therefore, the three activity experiments are conducted separately. In future experiments, the activity transitions will be included. In experiment trails, the speed is fixed along with slope of the treadmill. The speed change during experiments might have provided more insights into the study of human impedance modulation. In this study, the AIT approach is evaluated on healthy subjects and not on impaired subjects. It will be useful to observe the fuzzy likelihood profiles of gait and activity for impaired subjects.

In this paper, the AIT approach is designed to make it suitable for rehabilitation training in the indoor environment. The authors believe that the AIT have the potential for the applications in outdoors as well. However, the complexity of the problem increases in terms of gait speed, terrain conditions, and more activities.

8. Conclusion

In this paper, an online impedance tuning algorithm was proposed for a knee exoskeleton to provide personalized assistance based on simultaneous detection of activity and gait phase. Human knee impedance was characterized by collected walking data. The uncertainty of activity and gait phases was modeled with a fuzzy likelihood, and a GMM was developed to determine the desired robot impedance. The AIT was compared with CI and FSM approaches in a study with three participants. The AIT algorithm led to reduction of vastus medialis muscle activity, and it also yielded increased cadence and reduced step length in comparison to baseline approaches.

The future work will introduce transitions in activities as well. The AIT approach will be tested in outdoor environmental conditions. EMG sensors will be put on other muscles of

the leg to comprehensively study the effect of the impedance tuning, and patients will be recruited to evaluate the efficacy of AIT in assisting abnormal gaits.

Acknowledgement

This work was supported in part by the National Science Foundation under Grant IIS-1756031, and in part by Science Foundation Arizona under a Bisgrove Early Tenure-Track Faculty Award.

References

- J. M. Ortman, et al., An aging nation: the older population in the United States, United States Census Bureau, Economics and Statistics Administration, US Department of Commerce, 2014.
- [2] H. Gage, L. Storey, Rehabilitation for Parkinson's disease: a systematic review of available evidence, Clinical Rehabilitation 18 (5) (2004) 463– 482
- [3] A. M. Dollar, H. Herr, Lower extremity exoskeletons and active orthoses: challenges and state-of-the-art, IEEE Trans. Robot. 24 (1) (2008) 144– 158.
- [4] J. Bae, W. Zhang, M. Tomizuka, Network-based rehabilitation system for improved mobility and tele-rehabilitation, IEEE Trans. Control Syst. Technol. 21 (5) (2013) 1980–1987.
- [5] W. Zhang, M. Tomizuka, N. Byl, A wireless human motion monitoring system for smart rehabilitation, Journal of Dynamic Systems, Measurement, and Control 138 (11) (2016) 111004.
- [6] K. Kong, M. Tomizuka, A gait monitoring system based on air pressure sensors embedded in a shoe, IEEE/ASME Trans. Mechatronics 14 (3) (2009) 358–370.
- [7] Y. H. Yin, et al., Emg and epp-integrated human-machine interface between the paralyzed and rehabilitation exoskeleton, IEEE Trans. Inf. Technol. Biomed. 16 (4) (2012) 542–549.
- [8] S. Patel, et al., Monitoring motor fluctuations in patients with parkinson's disease using wearable sensors, IEEE Trans. Inf. Technol. Biomed. 13 (6) (2009) 864–873.
- [9] D. Trabelsi, et al., An unsupervised approach for automatic activity recognition based on hidden markov model regression, IEEE Trans. Autom. Sci. Eng 10 (3) (2013) 829–835.
- [10] K. Kong, J. Bae, M. Tomizuka, A compact rotary series elastic actuator for human assistive systems, IEEE/ASME Trans. Mechatronics 17 (2) (2012) 288–297.
- [11] J. F. Veneman, et al., A series elastic-and bowden-cable-based actuation system for use as torque actuator in exoskeleton-type robots, Int. J. Robotics Res. 25 (3) (2006) 261–281.
- [12] V. Grosu, et al., Design of smart modular variable stiffness actuators for robotic-assistive devices, IEEE/ASME Trans. Mechatronics 22 (4) (2017) 1777, 1785
- [13] P. Polygerinos, et al., Soft robotics: Review of fluid-driven intrinsically soft devices; manufacturing, sensing, control, and applications in humanrobot interaction, Advanced Engineering Materials.
- [14] N. Hogan, Impedance control: An approach to manipulation, in: American Control Conference, 1984, IEEE, 1984, pp. 304–313.
- [15] H. Kawamoto, Y. Sankai, Power assist method based on phase sequence and muscle force condition for hal, Advanced Robotics 19 (7) (2005) 717–734
- [16] G. Zeilig, H. Weingarden, M. Zwecker, I. Dudkiewicz, A. Bloch, A. Esquenazi, Safety and tolerance of the rewalk¢ exoskeleton suit for ambulation by people with complete spinal cord injury: A pilot study, The journal of spinal cord medicine 35 (2) (2012) 96–101.
- [17] S. A. Kolakowsky-Hayner, J. Crew, S. Moran, A. Shah, Safety and feasibility of using the ekso¢ bionic exoskeleton to aid ambulation after spinal cord injury, J Spine 4 (2013) 003.
- [18] T. C. Bulea, R. Kobetic, M. L. Audu, J. R. Schnellenberger, R. J. Triolo, Finite state control of a variable impedance hybrid neuroprosthesis for locomotion after paralysis, IEEE Transactions on Neural Systems and Rehabilitation Engineering 21 (1) (2013) 141–151.

- [19] A. J. del Ama, Á. Gil-Agudo, J. L. Pons, J. C. Moreno, Hybrid fes-robot cooperative control of ambulatory gait rehabilitation exoskeleton, Journal of neuroengineering and rehabilitation 11 (1) (2014) 27.
- [20] S. Wang, L. Wang, C. Meijneke, E. Van Asseldonk, T. Hoellinger, G. Cheron, Y. Ivanenko, V. La Scaleia, F. Sylos-Labini, M. Molinari, et al., Design and control of the mindwalker exoskeleton, IEEE transactions on neural systems and rehabilitation engineering 23 (2) (2015) 277–286.
- [21] H. A. Varol, F. Sup, M. Goldfarb, Multiclass real-time intent recognition of a powered lower limb prosthesis, IEEE Transactions on Biomedical Engineering 57 (3) (2010) 542–551.
- [22] B. E. Lawson, H. A. Varol, A. Huff, E. Erdemir, M. Goldfarb, Control of stair ascent and descent with a powered transfemoral prosthesis, IEEE Transactions on Neural Systems and Rehabilitation Engineering 21 (3) (2013) 466–473.
- [23] J. Li, B. Shen, C.-M. Chew, C. L. Teo, A. N. Poo, Novel functional task-based gait assistance control of lower extremity assistive device for level walking, IEEE Transactions on Industrial Electronics 63 (2) (2016) 1096–1106.
- [24] E. Perreault, L. Hargrove, D. Ludvig, H. Lee, J. Sensinger, Considering limb impedance in the design and control of prosthetic devices, in: Neuro-Robotics, Springer, 2014, pp. 59–83.
- [25] C. Tai, C. J. Robinson, Knee elasticity influenced by joint angle and perturbation intensity, IEEE Transactions on Rehabilitation Engineering 7 (1) (1999) 111–115.
- [26] S. Pfeifer, M. Hardegger, H. Vallery, R. List, M. Foresti, R. Riener, E. J. Perreault, Model-based estimation of active knee stiffness, in: Rehabilitation Robotics (ICORR), 2011 IEEE International Conference on, IEEE, 2011, pp. 1–6.
- [27] R. Ranzani, Adaptive human model-based control for active knee prosthetics, Master's thesis (2014).
- [28] P. T. Chinimilli, et al., Hysteresis compensation for ground contact force measurement with shoe-embedded air pressure sensors, in: ASME Dyn. Sys. Control Conf., 2016, p. V001T09A006.
- [29] J. Favre, et al., Functional calibration procedure for 3d knee joint angle description using inertial sensors, Journal of Biomechanics 42 (14) (2009) 2330–2335.
- [30] H. Ramakrishnan, G. Masiello, M. Kadaba, On the estimation of the three dimensional joint moments in gait, in: ASME Biomechanics Symposium, Vol. 120, 1991, pp. 333–339.
- [31] D. A. Winter, D. Robertson, Joint torque and energy patterns in normal gait, Biological Cybernetics 29 (3) (1978) 137–142.
- [32] G. Klir, B. Yuan, Fuzzy sets and fuzzy logic, Vol. 4, Prentice hall New Jersey, 1995.
- [33] P. T. Chinimilli, S. Redkar, W. Zhang, Human activity recognition using inertial measurement units and smart shoes, in: American Control Conference, 2017, pp. 1462–1467.
- [34] D. Reynolds, Gaussian mixture models, Encyclopedia of biometrics (2015) 827–832.
- [35] O. Unluhisarcikli, M. Pietrusinski, B. Weinberg, P. Bonato, C. Mavroidis, Design and control of a robotic lower extremity exoskeleton for gait rehabilitation, in: Intelligent Robots and Systems (IROS), 2011 IEEE/RSJ International Conference on, IEEE, 2011, pp. 4893–4898.
- [36] A. Burden, M. Trew, V. Baltzopoulos, Normalisation of gait emgs: a reexamination, Journal of Electromyography and Kinesiology 13 (6) (2003) 519–532.
- [37] R. Merletti, H. Hermens, Introduction to the special issue on the seniam european concerted action (2000).
- [38] K. Knaepen, et al., Human–robot interaction: Kinematics and muscle activity inside a powered compliant knee exoskeleton, IEEE Trans. Neural Syst. Rehabil. Eng. 22 (6) (2014) 1128–1137.
- [39] D. Aoyagi, W. E. Ichinose, S. J. Harkema, D. J. Reinkensmeyer, J. E. Bobrow, A robot and control algorithm that can synchronously assist in naturalistic motion during body-weight-supported gait training following neurologic injury, IEEE Transactions on Neural Systems and Rehabilitation Engineering 15 (3) (2007) 387–400.
- [40] E. H. Van Asseldonk, J. F. Veneman, R. Ekkelenkamp, J. H. Buurke, F. C. Van der Helm, H. van der Kooij, The effects on kinematics and muscle activity of walking in a robotic gait trainer during zero-force control, IEEE transactions on neural systems and rehabilitation engineering 16 (4) (2008) 360–370.